

Scenario analysis of livestock-related PM_{2.5} pollution based on a new heteroskedastic spatiotemporal model

Jacopo Rodeschini^{a,*}, Alessandro Fassò^b, Francesco Finazzi^b and Alessandro Fusta Moro^a

^aDepartment of Engineering and Applied Science (DISA), University of Bergamo, Via Pasubio 3, Dalmine (BG), 24044, Italy,

^bDepartment of Economics, University of Bergamo, Via dei Caniana 2, Bergamo, 24127, Italy,

ARTICLE INFO

Keywords:

PM_{2.5} concentrations
Scenario analysis
Ammonia emissions
Air quality
Lombardy Italy

ABSTRACT

The air in the Lombardy Plain, Italy, is one of the most polluted in Europe due to limited atmosphere circulation and high emission levels. There is broad scientific consensus that ammonia (NH₃) emissions have a primary impact on air quality, and, in Lombardy, the agricultural sector and livestock activities are widely recognised as being responsible for approximately 97% of regional ammonia emissions due to the high density of livestock.

In this paper, we quantify the relationship between ammonia emissions and PM_{2.5} concentrations in the Lombardy Plain and evaluate PM_{2.5} changes due to the reduction of ammonia emissions through a "what-if" scenario analysis. The information in the data is exploited using a spatiotemporal statistical model capable of handling spatial and temporal correlation, as well as missing data. To do this, we propose a new heteroskedastic extension of the well-established Hidden Dynamic Geostatistical Model. Maximum likelihood parameter estimates are obtained by the expectation-maximisation algorithm and implemented in a new version of the D-STEM software.

Considering the years between 2016 and 2020, the scenario analysis is carried out on high-resolution PM_{2.5} maps of the Lombardy Plain. As a result, it is shown that a 26% reduction in NH₃ emissions in the wintertime could reduce the PM_{2.5} average by 1.44 $\mu\text{g}/\text{m}^3$ while a 50% reduction could reduce the PM_{2.5} average by 2.76 $\mu\text{g}/\text{m}^3$ which corresponds to a reduction close to 3.6% and 7% respectively. Finally, results are detailed by province and land type.

1. Introduction

Air pollutants can be categorised into two groups: primary and secondary. Primary pollutants are those directly emitted into the atmosphere, while secondary pollutants are formed in the atmosphere through chemical reactions and microphysical processes involving precursor gases. Ammonia (NH₃) is a key precursor gas for secondary particulate matter (PM), specifically PM₁₀ and PM_{2.5}. In the Lombardy region, the primary sources of ammonia are livestock and fertilisers, accounting for approximately 97% of the overall regional emissions [3, 20, 21]. Although total annual NH₃ emissions remain relatively constant over the considered period, variations within the year are influenced by seasonal agricultural practices. In the Lombardy Plain, due to limited air circulation and stability in the air, PM_{2.5} frequently accumulates at hazardous concentrations, posing risks to human health. The elevated pollution levels in Lombardy Plain have led to one of the highest PM_{2.5}-related mortality rates in Europe, with 100-150 premature deaths per 100,000 inhabitants [8].

Using chemical transport model (CTM) simulations, several studies showed that within Europe, reducing NH₃ emissions stands out as one of the most efficient control strategies for mitigating PM_{2.5} levels in both summer and

winter seasons. In particular, [22] used five distinct control strategies, with a particular focus on testing a 50% reduction in gaseous emissions (SO₂, NH₃, NO_x and anthropogenic volatile organic compounds) to assess concentration sensitivity to emissions. The findings indicated that, in the majority of European regions, reducing NH₃ emissions during winter and summer periods proves more efficacious in lowering overall PM_{2.5} levels compared to reductions in other gas precursors. Moreover, [6] showed that a targeted 50% reduction in ammonia emissions results in a decrease of total PM_{2.5} levels by up to 2.4 $\mu\text{g}/\text{m}^3$ in the Lombardy region. Additionally, [29] demonstrated that the nonlinear behaviour of the sulphate-nitrate-ammonia system influences the efficacy of PM_{2.5} control strategies.

Our study differs from the above literature, as we use a statistical spatiotemporal model to perform a "what-if" scenario analysis assessing the reduction in PM_{2.5} concentration due to certain ammonia emission reduction scenarios. In [9], the statistical relation between observed PM_{2.5} and NH₃ concentrations is modelled using a generalised least square approach able to handle spatial and temporal correlation. This is based on the five monitoring stations in Lombardy where observed concentrations of both substances are available.

Unfortunately, the Lombardy air quality monitoring network is not specifically designed to monitor agricultural air pollutants. Most monitoring stations are located in areas with low NH₃ emission levels, and none are located where such emissions reach the highest peaks. Consequently, only very few NH₃ concentration stations are available in the Lombardy region, and a fully spatiotemporal model is not

*Corresponding author

✉ jacopo.rodeschini@unibg.it (J. Rodeschini);

alessandro.fasso@unibg.it (A. Fassò); francesco.finazzi@unibg.it (F. Finazzi); alessandro.fustamoro@unibg.it (A. Fusta Moro)

ORCID(s): 0000-0003-1874-1854 (J. Rodeschini); 0000-0001-5132-9488 (A. Fassò); 0000-0002-1295-7657 (F. Finazzi); 0000-0003-1129-5038 (A. Fusta Moro)

viable on those data. Moreover, such network spatial unbalance may imply a preferential sampling bias.

Over the last few decades, significant progress has been made in spatiotemporal statistical models in general [5, 15, 19, 31], and for air quality in particular [2, 37, 36]. A well-established framework to study spatiotemporal processes is the state space model and the related Kalman filter technique [2, 10, 16, 28, 30]. In this context, [2] proposes a multivariate spatiotemporal statistical model named the Hidden Dynamic Geostatistical Model (HDGM), which is a two-level hierarchical model suitable for complex environmental processes. In [27], the HDGM has been compared with the Generalised Additive Mixed Model and the Random Forest with Residual Kriging, in PM_{2,5} modelling in Lombardy. The HDGM demonstrated better performance in cross-validation. In addition, considering the heteroskedasticity, the authors point out that model uncertainty varies throughout the year for all three models, and PM_{2,5} concentrations in winter can be predicted less accurately than in summer.

In spatiotemporal models, heteroskedasticity has various facets and may refer to time, space, data heterogeneity or a mixture of the three. Also, the skedastic function may be deterministic or stochastic. An example of data heterogeneity arises in data fusion problems where the data vector elements are obtained by different sensors or processes. See, e.g., [33].

Considering the temporal dimension, we may model stochastic heteroskedasticity using the well-known approach introduced by the Nobel Prize Robert F. Engle [7]. It is based on conditioning the error variance on the past and resulted in the large suite of GARCH-like models developed in the last decades. See, e.g., [13]. Also, the approach based on a deterministic skedastic function is used in environmental statistics, for example, a seasonal variance. See, e.g., [1, 9].

Considering the spatial dimension, deterministic spatial skedastic functions have been used extensively. For example, it is considered by [23] in spatial econometrics models and by [17] in ecology. Also, Engle and Bollerslev's generalised conditionally heteroskedastic approach has been recently introduced to spatial econometrics by [26]. For a review and developments, see [25] and references therein.

In our study, we are not interested in modelling and interpreting the skedastic function per se but as a nuisance parameter needed to make correct inferences on spatial maps and aggregated results. For these reasons, we opt for a very flexible unstructured time-varying error variance applied to the HDGM. This results in a high-dimensional parameter dimension, which is efficiently handled by the expectation-maximisation (EM) algorithm.

The rest of the paper is organised as follows. Section 2 discusses the methodology adopted. In particular Section 2.1 defines the heteroskedastic HDGM and the maximum likelihood estimation algorithm. Section 2.5 presents the "what-if" scenario analysis approach and provides the formula to compute the impact uncertainty; Section 3 addresses the application of the heteroskedastic HDGM to the observed daily PM_{2,5} in the Lombardy Region, between 2016 and

2020, and outlines the scenario analysis to assess the PM_{2,5} changes due to NH₃ emissions; the results are summarised in Section 4. The Conclusions Section closes the paper.

2. Methodology

Despite the HDGM's capability to handle multivariate spatiotemporal data, this study focuses on the univariate case. In particular, the next section introduces the heteroskedastic HDGM to estimate PM_{2,5} concentrations based on the data observed within the air quality monitoring network.

2.1. The Heteroskedastic Hidden Dynamic Geostatistical Model

To understand the relationship between predictors and the response variable, taking into account spatial and temporal correlation, we propose a heteroskedastic extension of the univariate HDGM [2, 4] which is a two-level hierarchical model. The hierarchy is constructed by putting together two conditional submodels. At the first level, the observation variability is modelled by the measurement equation, which is essentially given by a regression component, a stochastic latent variable, and an error with time-varying variance. The latent variable is defined at the second level of the hierarchy. It handles the spatiotemporal correlation through a Markovian process. The innovation term is a zero-mean Gaussian process with a spatial covariance function.

Let $y(\mathbf{s}, t)$ be the response variable observed at site $\mathbf{s} \in \mathbb{S}^2$, where \mathbb{S}^2 is the surface of the sphere embedded in \mathbb{R}^3 , and discrete time $t = 1, \dots, T$. The heteroskedastic univariate HDGM is defined as follows:

$$\begin{aligned} y(\mathbf{s}, t) &= \mathbf{x}'(\mathbf{s}, t)\boldsymbol{\beta} + \alpha z(\mathbf{s}, t) + \epsilon(\mathbf{s}, t) \\ z(\mathbf{s}, t) &= gz(\mathbf{s}, t-1) + \eta(\mathbf{s}, t). \end{aligned} \quad (1)$$

The $\boldsymbol{\beta}$ is a vector of fixed effect coefficients; $\mathbf{x}(\mathbf{s}, t)$ is a $p \times 1$ vector of covariates that accounts for all exogenous effects; α is a scale parameter of the latent variable; the heteroskedastic measurement error $\epsilon(\mathbf{s}, t) \sim N(0, \sigma_{\epsilon,t}^2)$ is independent in space and time; $z(\mathbf{s}, t)$ is a unit-variance Markovian scalar process ruled by the transition coefficient g ; the innovation term $\eta(\mathbf{s}, t)$ is a zero-mean Gaussian process, $GP(0, \rho(\|\mathbf{s} - \mathbf{s}'\|; \theta))$, independent in time where ρ is a valid spatial correlation function and $\|\mathbf{s} - \mathbf{s}'\|$ is the geodetic distance between \mathbf{s} and $\mathbf{s}' \in \mathbb{S}^2$. The model parameters set is $\boldsymbol{\Psi} = \{\boldsymbol{\beta}, g, \theta, \alpha, \sigma_{\epsilon,1}^2, \dots, \sigma_{\epsilon,T}^2\}$ which is estimated using the maximum likelihood (ML) estimation through the EM algorithm.

2.2. Matrix representation of univariate heteroskedastic HDGM

Using the same notation introduced in [2], suppose that the variable $y(\mathbf{s}, t)$ is observed at each spatial location $\mathbf{S}_n = \{\mathbf{s}_1, \dots, \mathbf{s}_n\}$. Let $\mathbf{y}_t = (y(\mathbf{s}_1, t), \dots, y(\mathbf{s}_n, t))'$ be the $n \times 1$ vector of the response. With these assumptions, the process can be considered as a classical state-space model [32] where the

observations at time t follow the equations:

$$\begin{aligned} \mathbf{y}_t &= \mathbf{X}_t \boldsymbol{\beta} + \alpha \mathbf{z}_t + \boldsymbol{\epsilon}_t \\ \mathbf{z}_t &= g \mathbf{z}_{t-1} + \boldsymbol{\eta}_t \end{aligned} \quad (2)$$

with $\mathbf{X}_t = (\mathbf{x}(s_1, t), \dots, \mathbf{x}(s_n, t))'$. Vectors \mathbf{z}_t and $\boldsymbol{\eta}_t$ are defined similarly to \mathbf{y}_t . Moreover, $\boldsymbol{\epsilon}_t$ is a n -dimensional random noise vector, $\boldsymbol{\epsilon}_t \sim N_n(\mathbf{0}, \boldsymbol{\Sigma}_{\epsilon,t})$ where $\boldsymbol{\Sigma}_{\epsilon,t}$ is given by $\boldsymbol{\Sigma}_{\epsilon,t} = \sigma_{\epsilon,t}^2 \mathbf{I}_n$, and \mathbf{I}_n is the identity matrix of order n . The distribution of the latent variable at $t = 0$, $\mathbf{z}_0 \sim N_n(\boldsymbol{\mu}_0, \boldsymbol{\Sigma}_0)$. If all parameters in $\boldsymbol{\Psi}$ are known, the unobserved temporal process \mathbf{z}_t in the model (2) is estimated for each time t through the Kalman smoother technique, initialised with the condition \mathbf{z}_0 . Specifically, the Kalman smoother yields the state estimate $\mathbf{z}_t^T = E_{\boldsymbol{\Psi}}(\mathbf{z}_t | \mathbf{Y})$ and the corresponding uncertainty $\mathbf{P}_t^T = \text{Var}_{\boldsymbol{\Psi}}(\mathbf{z}_t | \mathbf{Y})$. The Kalman smoother algorithm handles in a natural way time-varying parameters [32]. Alongside the Kalman smoother output, the quantities \mathbf{S}_{10} , \mathbf{S}_{00} , and \mathbf{S}_{11} are introduced as the so-called EM second moments [32].

2.3. Complete-data likelihood

From the model assumptions, we have the following probability distributions:

$$\begin{aligned} \mathbf{y}_t | \mathbf{z}_t &\sim N_n(\boldsymbol{\mu}_t, \boldsymbol{\Sigma}_{\epsilon,t}) \\ \mathbf{z}_t | \mathbf{z}_{t-1} &\sim N_n(g \mathbf{z}_{t-1}, \boldsymbol{\Sigma}_{\eta}) \end{aligned}$$

where $\boldsymbol{\mu}_t = \mathbf{X}_t \boldsymbol{\beta} + \alpha \mathbf{z}_t$. Following the results in Appendix A.1 of [2] and assuming that $\boldsymbol{\Sigma}_{\epsilon,t}$ is positive defined, the complete-data log-likelihood function for observations $\mathbf{Y} = \{\mathbf{y}_1, \dots, \mathbf{y}_T\}$ and $\mathbf{Z} = \{\mathbf{z}_0, \mathbf{z}_1, \dots, \mathbf{z}_T\}$ is given by

$$\begin{aligned} -2l(\boldsymbol{\Psi}; \mathbf{Y}, \mathbf{Z}) &= \sum_{t=1}^T \log |\boldsymbol{\Sigma}_{\epsilon,t}| + \sum_{t=1}^T \mathbf{e}_t' \boldsymbol{\Sigma}_{\epsilon,t}^{-1} \mathbf{e}_t \\ &+ \log |\boldsymbol{\Sigma}_0| + (\mathbf{z}_0 - \boldsymbol{\mu}_0)' \boldsymbol{\Sigma}_0^{-1} (\mathbf{z}_0 - \boldsymbol{\mu}_0) \\ &+ T \log |\boldsymbol{\Sigma}_{\eta}| + \sum_{t=1}^T (\mathbf{z}_t - g \mathbf{z}_{t-1})' \boldsymbol{\Sigma}_{\eta}^{-1} (\mathbf{z}_t - g \mathbf{z}_{t-1}) \end{aligned} \quad (3)$$

where $\mathbf{e}_t = \mathbf{y}_t - \boldsymbol{\mu}_t$ and $|\cdot|$ is the matrix determinant. Due to the additive structure of Eq. (3) where the right-hand terms depend on different subsets of the parameters, $l(\boldsymbol{\Psi}; \mathbf{Y}, \mathbf{Z})$ can be written as $l(\boldsymbol{\Psi}) = l(\boldsymbol{\Psi}_1) + l(\boldsymbol{\Psi}_0) + l(\boldsymbol{\Psi}_2)$ where $\boldsymbol{\Psi}_1 = \{\alpha, \boldsymbol{\beta}, \sigma_{\epsilon,1}^2, \dots, \sigma_{\epsilon,T}^2\}$, $\boldsymbol{\Psi}_0 = \{\boldsymbol{\mu}_0, \boldsymbol{\Sigma}_0\}$ and $\boldsymbol{\Psi}_2 = \{\theta, g\}$.

2.4. Estimation formulas

The ML estimation of the unknown parameter vector $\boldsymbol{\Psi}$ is performed using the iterates EM algorithm. At each iteration, there are two steps, the E-step and the M-step. The E-step finds the conditional expectation of the complete-data log-likelihood given the observation, namely

$$Q(\boldsymbol{\Psi}, \boldsymbol{\Psi}^{(m)}) = E_{\boldsymbol{\Psi}^{(m)}}(-2l(\boldsymbol{\Psi}; \mathbf{Y}, \mathbf{Z}) | \mathbf{Y})$$

where $E_{\boldsymbol{\Psi}^{(m)}}$ is the expectation given the parameter estimate at iteration m . At the M-step, $Q(\boldsymbol{\Psi}, \boldsymbol{\Psi}^{(m)})$ is maximised

with respect to $\boldsymbol{\Psi}$ and the new estimate is $\boldsymbol{\Psi}^{(m+1)} = \text{argmax}_{\boldsymbol{\Psi}} Q(\boldsymbol{\Psi}, \boldsymbol{\Psi}^{(m)})$. Due to the linear properties of the conditional expectation we can write $Q(\boldsymbol{\Psi}, \boldsymbol{\Psi}^{(m)}) = Q(\boldsymbol{\Psi}_1, \boldsymbol{\Psi}^{(m)}) + Q(\boldsymbol{\Psi}_0, \boldsymbol{\Psi}^{(m)}) + Q(\boldsymbol{\Psi}_2, \boldsymbol{\Psi}^{(m)})$. In this way, the maximisation step can be broken into several smaller optimisation problems.

In the following, let $E(\cdot | \cdot) \equiv E_{\boldsymbol{\Psi}^{(m)}}(\cdot | \cdot)$ and $\text{Var}(\cdot | \cdot) \equiv \text{Var}_{\boldsymbol{\Psi}^{(m)}}(\cdot | \cdot)$. Moreover, $\boldsymbol{\mu}_0 \equiv \boldsymbol{\mu}_0^{(m)}$, $\boldsymbol{\Sigma}_0 \equiv \boldsymbol{\Sigma}_0^{(m)}$, $g \equiv g^{(m)}$, $\boldsymbol{\Sigma}_{\epsilon,t} \equiv \boldsymbol{\Sigma}_{\epsilon,t}^{(m)}$ and $\boldsymbol{\Sigma}_{\eta} \equiv \boldsymbol{\Sigma}_{\eta}^{(m)}$ that is, vectors and matrices are evaluated using the estimate parameters at iteration m of the EM algorithm.

The $Q(\boldsymbol{\Psi}_i, \boldsymbol{\Psi}^{(m)})$ term for $i = 0, 1, 2$ is expressed as:

$$\begin{aligned} Q(\boldsymbol{\Psi}_1, \boldsymbol{\Psi}^{(m)}) &= \sum_{t=1}^T \log |\boldsymbol{\Sigma}_{\epsilon,t}| \\ &+ tr \left(\sum_{t=1}^T E(\mathbf{e}_t | \mathbf{Y})' \boldsymbol{\Sigma}_{\epsilon,t}^{-1} E(\mathbf{e}_t | \mathbf{Y}) + \boldsymbol{\Sigma}_{\epsilon,t}^{-1} \text{Var}(\mathbf{e}_t | \mathbf{Y}) \right) \end{aligned}$$

$$\begin{aligned} Q(\boldsymbol{\Psi}_0, \boldsymbol{\Psi}^{(m)}) &= \log |\boldsymbol{\Sigma}_0| \\ &+ tr \left[\boldsymbol{\Sigma}_0^{-1} \left(E(\mathbf{z}_0 | \mathbf{Y}) - \boldsymbol{\mu}_0 \right) \left(E(\mathbf{z}_0 | \mathbf{Y}) - \boldsymbol{\mu}_0 \right)' + \text{Var}(\mathbf{z}_0 | \mathbf{Y}) \right] \end{aligned}$$

$$Q(\boldsymbol{\Psi}_2, \boldsymbol{\Psi}^{(m)}) = T \log |\boldsymbol{\Sigma}_{\eta}| + tr \left[\boldsymbol{\Sigma}_{\eta}^{-1} \left(\mathbf{S}_{11} - 2g \mathbf{S}_{10} + g^2 \mathbf{S}_{00} \right) \right]$$

where $E(\mathbf{e}_t | \mathbf{Y})$ and $\text{Var}(\mathbf{e}_t | \mathbf{Y})$ are given in Appendix A.1 and Appendix A.2 of [2] respectively. The maximisation step for updating $\boldsymbol{\Psi}_i$ is derived by solving

$$\frac{\partial}{\partial \boldsymbol{\Psi}_i} Q_i(\boldsymbol{\Psi}_i, \boldsymbol{\Psi}^{(m)}) = 0.$$

As a result, starting with initial value $\boldsymbol{\Psi}^{(0)}$, the updating formulas are:

$$(\sigma_{\epsilon,t}^2)^{(m+1)} = \frac{1}{n} tr(\boldsymbol{\Omega}_t^{(m)}) \quad (4)$$

$$\begin{aligned} \boldsymbol{\beta}^{(m+1)} &= \left[\sum_{t=1}^T (\mathbf{X}_t)' (\boldsymbol{\Sigma}_{\epsilon,t}^{(m)})^{-1} \mathbf{X}_t \right]^{-1} \\ &\left[\sum_{t=1}^T (\mathbf{X}_t)' (\boldsymbol{\Sigma}_{\epsilon,t}^{(m)})^{-1} (\mathbf{y}_t - \alpha^{(m)} \mathbf{z}_t^{T,(m)}) \right] \end{aligned} \quad (5)$$

$$\begin{aligned} \alpha^{(m+1)} &= \sum_{t=1}^T tr \left[\mathbf{z}_t^{T,(m)} (\boldsymbol{\Sigma}_{\epsilon,t}^{(m)})^{-1} (\mathbf{y}_t - \mathbf{X}_t \boldsymbol{\beta}^{(m)}) \right] \\ &\left(\sum_{t=1}^T tr \left[(\boldsymbol{\Sigma}_{\epsilon,t}^{(m)})^{-1} \left(\mathbf{z}_t^{T,(m)} (\mathbf{z}_t^{T,(m)})' + \mathbf{P}_t^{T,(m)} \right) \right] \right)^{-1} \end{aligned} \quad (6)$$

$$\boldsymbol{\mu}_0^{(m+1)} = \mathbf{z}_0^{T,(m)} \quad (7)$$

$$\Sigma_0^{(m+1)} = \mathbf{P}_0^{T,(m)} \quad (8)$$

$$g^{(m+1)} = \text{tr}(\mathbf{S}_{10}^{(m)}) \text{tr}(\mathbf{S}_{00}^{(m)})^{-1} \quad (9)$$

$$\begin{aligned} \theta^{(m+1)} = \underset{\theta}{\text{argmax}} & \left(T \log |\Sigma_{\eta}^{(m)}| \right. \\ & \left. + \text{tr} \left[(\Sigma_{\eta}^{(m)})^{-1} \left(\mathbf{S}_{11}^{(m)} - 2g^{(m)} \mathbf{S}_{10}^{(m)} + (g^{(m)})^2 \mathbf{S}_{00}^{(m)} \right) \right] \right) \end{aligned} \quad (10)$$

where $\Omega_t^{(m)} = E(e_t|Y)E(e_t|Y)' + \text{Var}(e_t|Y)$ is given in Appendix A.3 of [2]. Note that the updating formulas (4) to (10), are similar to those provided by [2]. The main exception lies in the parameters in Ψ_0 which defines the measurement equation and undergoes modification due to the introduction of time-varying variance. Specifically, Eq. (4) results in an average over space for each time t . The updating formulas for β and α , in Eqs. (5) and (6) respectively, take into account the time-varying variance $\Sigma_{e,t}$.

Given the ML estimate $\hat{\Psi}$, predictions of the response variable at new sites s_0 and time $t = 1, \dots, T$ are given by

$$\hat{y}(s_0, t) = \mathbf{x}'(s_0, t) \hat{\beta} + \hat{\alpha}_z^T(s_0). \quad (11)$$

2.5. Scenario analysis approach

This section presents the scenario analysis approach adopted to assess the PM_{2.5} sensitivity to the NH₃ emissions. We consider the "What-if" scenario analysis approach: "What would happen if the NH₃ reductions were fully implemented at time 0 (1st January 2016)?" We compare the predicted PM_{2.5}, $\hat{y}(s, t)$, based on the observed NH₃ emissions with a prediction, $\hat{y}^r(s, t)$ where the NH₃ emissions are reduced by a factor r . The daily PM_{2.5} change $\Delta_y(s, t) = y(s, t) - y^r(s, t)$ and its variance are estimated by

$$\begin{aligned} \Delta_{\hat{y}}(s, t) &= \hat{y}(s, t) - \hat{y}^r(s, t) \\ \text{Var}(\Delta_{\hat{y}}(s, t) - \Delta_y(s, t)) &= \Delta_x' \Sigma_{\hat{\beta}} \Delta_x + \text{Var}(\epsilon_t - \epsilon_t^r) \end{aligned}$$

where $\Delta_x = \mathbf{x}(s, t) - \mathbf{x}^r(s, t)$; $\Sigma_{\hat{\beta}}$ is the estimate of the $\hat{\beta}$ covariance matrix; ϵ_t and ϵ_t^r are the measurement errors of both predictions which are independent and with the same variance. The average of the daily $\Delta_{\hat{y}}(s, t)$ and its variance over space subset \mathcal{D} and time interval \mathcal{I} are given by

$$\bar{\Delta}_{\hat{y}} = \frac{1}{\mathcal{D}^* \mathcal{I}^*} \sum_{s \in \mathcal{D}} \sum_{t \in \mathcal{I}} \Delta_{\hat{y}}(s, t) \quad (12)$$

$$\text{Var}(\bar{\Delta}_{\hat{y}} - \bar{\Delta}_y) = \bar{\Delta}_x' \Sigma_{\hat{\beta}} \bar{\Delta}_x + \frac{2}{(\mathcal{I}^*)^2 \mathcal{D}^*} \sum_{t \in \mathcal{I}} \hat{\sigma}_{\epsilon,t}^2 \quad (13)$$

where \mathcal{D}^* and \mathcal{I}^* are the number of pixels and days involved in the average computation; $\hat{\sigma}_{\epsilon,t}^2$ is the estimate of the variance of the measurement error and $\bar{\Delta}_x$ is the average of the design matrix. The Eq. (13) provides the standard deviation (std) used to assess the estimate change uncertainty in the next session.

3. Lombardy case study

In this section, the methodology discussed in Section 2 is used to estimate the impact of NH₃ emissions on the concentration of PM_{2.5} in the Lombardy Plain. The dataset description and preliminary analysis are detailed in Section 3.1 and Section 3.2, while the model estimation is described in Section 3.3. Finally, Section 3.4 discuss the scenario analysis implementation, details the result and provides maps of the PM_{2.5} change.

3.1. Data description

Our research is based on the Agrimonia dataset [12], which is a comprehensive daily spatiotemporal dataset for modelling the air quality of the Lombardy region. This dataset is open access and is available through the Zenodo repository [11]. It covers the period from 2016 to 2021 and includes daily concentrations of air pollutants, meteorological conditions, emission fluxes, land use, and livestock densities. Because spatiotemporal methods can benefit from neighbouring information to improve prediction performance near boundaries, the dataset also provides data for an area around the Lombardy region, obtained by applying a 0.3° buffer around regional boundaries.

We consider the period between 2016 and 2020 and the following variables: PM_{2.5} measured at 45 ground stations (30 of which belong to the Lombardy region, while the remaining 15 are located in the neighbouring area), wind speed (average wind speed at 100 m), temperature (air temperature at 2 m), relative humidity (RH), boundary layer height (BLH, maximum daily air mixing layer height), high vegetation index (HVI, high vegetation abundance), sulphur dioxide emissions (SO₂), total ammonia emissions from agriculture (NH₃), and nitrogen oxide emissions (NO_x).

In addition, we create new binary variables: Rain = 1 if the total daily precipitation exceeds the threshold of 1 mm, Urban = 1 if land use is classified as urban, and a new categorical variable Season which takes four categories: *Winter*, *Spring*, *Summer*, and *Autumn*. Table 1 summarises the variables used in this study along with the main statistics.

3.2. Preliminary analysis

It is well-noted that the air quality data are characterised by a seasonal pattern [20, 27]. In particular, the PM_{2.5} concentrations are higher in winter, due to meteorological conditions that reduce air circulation. The NO_x emissions follow human activities and during the cold months reach high levels of emissions due to endothermic-powered vehicles and domestic heating systems. Vice versa the seasonal behaviour of the NH₃ emissions is determined by seasonal practices of agricultural activities responsible for strong variations in NH₃ emissions level. In particular, the NH₃ emissions are higher in the Spring and Summer periods. Table 2 summarises the daily temperature average, emissions flow, and PM_{2.5} by season showing the composition regimes in the atmosphere.

The spatiotemporal variogram [4] in Figure 1 highlights strong spatial and temporal correlation, as it shows that the

Table 1

Variables selected from the Agrimonia dataset [12] and main descriptive statistics. The Rain and Urban variables are binary. Season is not included because it is a categorical variable.

Name	min	mean	max	std
PM _{2.5} [$\mu\text{g}/\text{m}^3$]	1.00	21.58	182.00	16.63
Wind speed [m/s]	0.56	2.59	11.93	1.33
Temperature [$^\circ\text{C}$]	-11.94	13.44	32.88	7.98
RH [%]	25.87	74.34	99.10	12.26
BLH [m]	27.38	1043.91	4420	556.77
HVI [m^2/m^2]	0.86	2.23	5.03	0.70
SO ₂ [$\text{mg}/(\text{m}^2\text{day})$]	0.05	3.34	45.06	5.53
NH ₃ [$\text{mg}/(\text{m}^2\text{day})$]	0.13	11.55	72.03	12.00
NO _x [$\text{mg}/(\text{m}^2\text{day})$]	0.75	14.06	118.60	16.73
Rain	0	0.02	1	0.15
Urban	0	0.75	1	0.43

Table 2

Seasonal average of daily Temperature [$^\circ\text{C}$], NH₃, NO_x and SO₂ emissions [mg/m^2] and PM_{2.5} concentrations [$\mu\text{g}/\text{m}^3$].

Season	Temperature	NH ₃	NO _x	SO ₂	PM _{2.5}
Winter	3.88	5.21	19.97	4.11	35.87
Spring	12.67	17.45	11.33	2.98	16.54
Summer	23.23	14.71	10.45	2.80	12.19
Autumn	13.83	8.70	14.59	3.46	21.62

variance increases with distance in both space and time. The temporal dynamics was further analysed through the partial autocorrelation function, which highlights the first lag (1 day) as the most significant autocorrelated component, indicating that a model with first-order Markovian dynamics is appropriate. The autocorrelation at lag one is close to 0.8 for all stations and suggests that PM_{2.5} is relatively stable in the atmosphere.

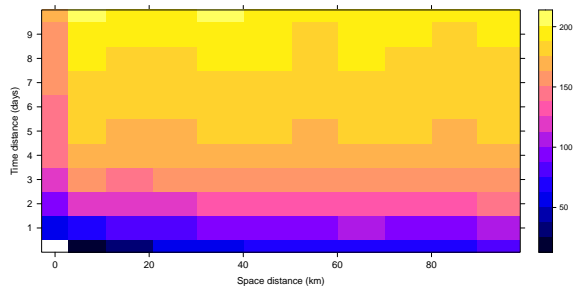


Figure 1: Spatiotemporal variogram computed on PM_{2.5} daily observations at 45 stations from 2016 to 2020.

A special focus is devoted to NH₃ emissions. The daily emission flux included in the Agrimonia dataset was provided monthly by the Copernicus Atmosphere Monitoring Service [18]. The spatial distribution of annual NH₃ emissions in 2020 is shown in Figure 2. The annual NH₃ emissions in 2020 aggregated by province are summarised

Table 3

Total NH₃ emissions by province in 2020.

Province	Province code	NH ₃ [t/year]
Bergamo	BG	7546
Brescia	BS	29524
Como	CO	1517
Cremona	CR	16892
Lecco	LC	615
Lodi	LO	6552
Mantua	MN	20336
Milan	MI	14013
Monza and Brianza	MB	714
Pavia	PV	8199
Sondrio	SO	4601
Varese	VA	1052

in Table 3. In particular, the provinces of Brescia, Cremona, and Mantua are characterised by higher emissions.

It is worth noting that the air quality monitoring network is not specifically designed to monitor ammonia emissions. Indeed, most monitoring stations are located in areas with low NH₃ emission levels and none are located where they reach the highest peaks, as shown in Figure 2. Raising potential issues of preferential spatial sampling bias which is briefly discussed later in Section 5.

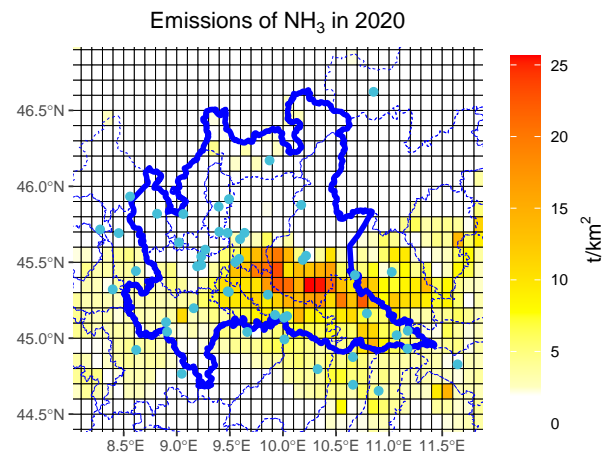


Figure 2: Annual NH₃ emissions (t/km^2) over the augmented Lombardy region in 2020. The cyan circles represent air quality stations. The continuous blue line represents the boundary of the Lombardy region while the dotted ones represent the province boundaries.

3.3. Estimated model

Given the extensive literature on air quality in the Lombardy region, we rely on these studies to select the covariates for the model (1). Specifically, [27] provides detailed insights into the impact of weather conditions on PM_{2.5} formation in Lombardy, while [9] explores the seasonality of pollutant concentration, revealing that the sensitivity of

PM_{2.5} to NH₃ and NO_x varies with Season. Based upon these findings, we adopt a univariate HDGM with a regression term specified as follows

$$PM_{2.5} \sim (\text{Intercept}) + \text{Windspeed} + \text{Temperature} \\ + \text{RH} + \text{Rain} + \text{BLH} + \text{Urban} + \text{HVI} + \text{SO}_2 \\ + \text{NO}_x + \text{NH}_3 + (\text{NO}_x + \text{NH}_3) : \text{Season}$$

while the spatial correlation function of the innovation term for the model (1) is defined by the exponential function as $\rho(\|s - s'\|; \theta) = \exp\{-\|s - s'\|/\theta\}$.

To avoid numerical issues, the response variable and covariates are standardised. So, the estimated parameters in the current subsection refer to this standardised setup. Table 4 summarises the estimated coefficients β of the linear regression model used for the large-scale component. All coefficients except the intercept are statistically significant. As expected, the role of NH₃ is most prominent in winter, when NH₃ plays a limiting role in the formation of PM_{2.5}. The estimated parameters of the latent variable and the uncertainty associated with them are $\hat{\theta} = 2.26^\circ$ ($std < 0.06^\circ$), $\hat{g} = 0.79$ ($std < 0.01$) and $\hat{\alpha} = 0.18$ ($std < 0.01$). Note that the latent process is stationary and the magnitude of g indicates that the $z(s, t)$ change smoothly over time. Finally, Figure 3 shows the daily $\hat{\sigma}_{\epsilon,t}^2$ which is higher in winter than in summer, and highlights the need for a heteroskedastic model.

We validate the model by considering its performance in Cross-Validation (CV). In particular, we use the Leave-One-Station-Out CV scheme (LOSOCV), a variation of the commonly used leave-one-out CV approach applied in the spatiotemporal framework [24]. To do this, we only use the 30 stations belonging to Lombardy in the LOSOCV procedure while the remaining 15 stations are used in the training set only. As a result, the model in-sample Root Mean Square Error (RMSE) is $3.85 \mu\text{g}/\text{m}^3$ while the CV-RMSE is $5.91 \mu\text{g}/\text{m}^3$, which improves the CTM performance [34].

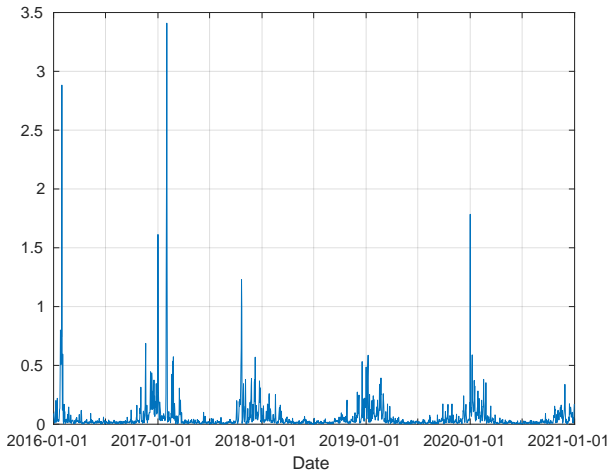


Figure 3: Estimated error variance, $\hat{\sigma}_{\epsilon,t}^2$.

In Figure 4, the distributions of the studentised residuals, computed as $e_t/\hat{\sigma}_{\epsilon,t}$, grouped by station are shown

Table 4

Estimate of the fixed effect coefficients of the model (1). $|t|$ is the absolute value of the t -statistic.

Name	β	std	$ t $	p-value
(Intercept)	-0.02	0.05	0.46	0.64
Wind speed	-0.08	0.00	23.87	0
Temperature	-0.21	0.02	10.63	0
RH	0.09	0.01	17.39	0
Rain	-0.01	0.00	2.87	4.10E-03
BLH	-0.07	0.00	14.87	0
Urban	-0.08	0.01	15.24	0
HVI	-0.03	0.00	6.88	0
SO2	-0.05	0.01	9.13	0
NO _x	0.10	0.01	10.95	0
NO _x :Winter	0.03	0.01	3.35	7.96E-04
NO _x :Summer	-0.02	0.01	3.88	1.06E-04
NO _x :Spring	-0.02	0.01	4.06	4.96E-05
NH ₃	0.11	0.01	8.96	0
NH ₃ :Winter	0.09	0.01	12.07	0
NH ₃ :Summer	-0.07	0.01	6.34	0
NH ₃ :Spring	-0.10	0.01	7.87	0

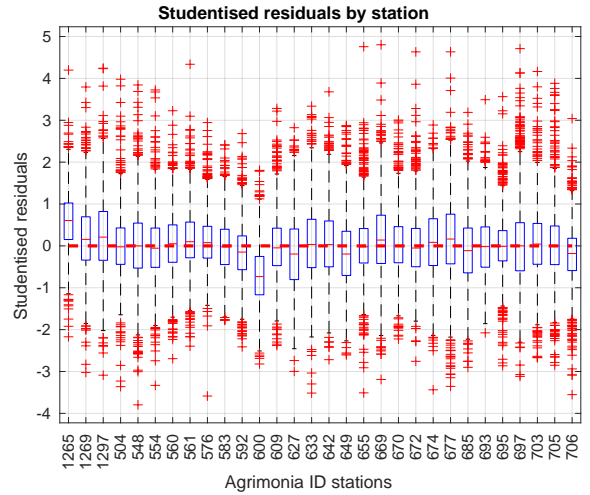


Figure 4: Studentised residuals grouped by station. The outliers (red cross) are identified by the Whisker length based on the first and third quartiles.

through boxplots. Their distributions are approximately centred around zero and moderately non-Gaussian. The residuals are further investigated through the Autocorrelation Function (ACF). We compute the ACF by station and then we summarise the autocorrelation coefficients for all stations by using the boxplot representation, as shown in Figure 5. The ACF is generally not significant except at lag one where there is a weak autocorrelation. This is not further considered as its influence in Eq. (13) is negligible.

3.4. Scenario Analysis

According to [34] we propose two different scenarios for NH₃ emissions reduction: (i) scenario named PRIA that accounts for a reduction of 26% in NH₃ emission; (ii) scenario named Strong that is characterised by a reduction of

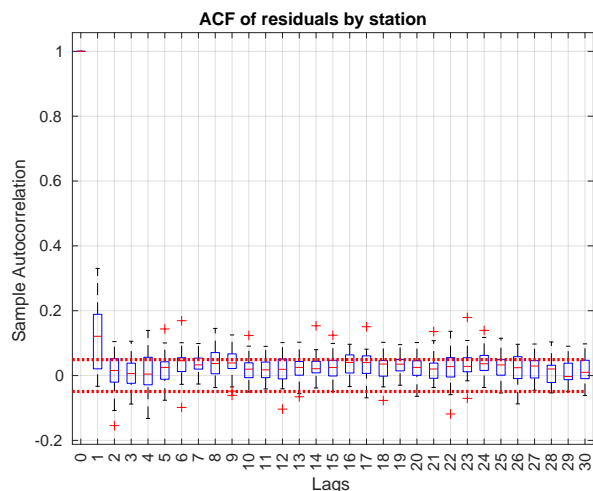


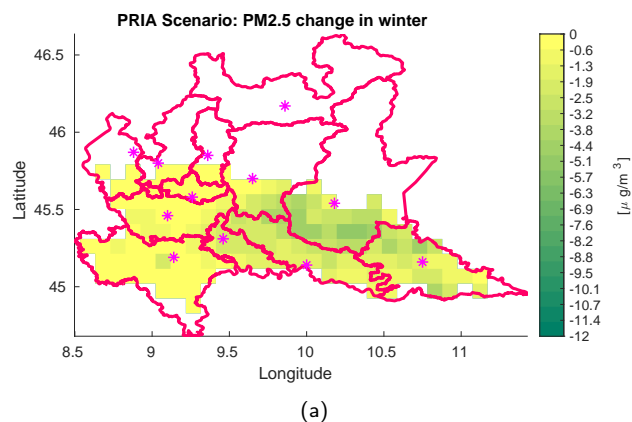
Figure 5: Autocorrelation Function (ACF) computed by station residuals for the first 30 lags (days) and summarised through boxplots. The outliers (red cross) are identified by the Whisker length based on the first and third quartiles.

50% in ammonia emissions. The PRIA scenario is based on the PRIA plan (in Italian "Piano Regionale degli Interventi per la qualità dell'Aria"), which identifies the actions needed to reduce ammonia emissions by 26% in Lombardy.

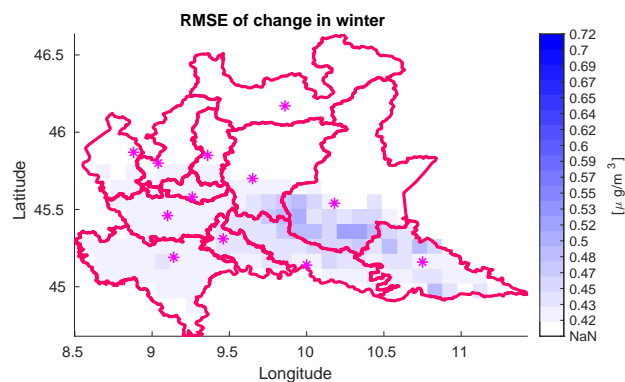
We consider the "What-if" scenario analysis approach: "What would happen if the NH₃ reductions were fully implemented at time 0 (1st January 2016)?" Considering the distribution of NH₃ emissions shown in Figure 2, we assess the scenario analysis only in non-forested areas below 640 m altitude. The results are back-transformed to the original units.

For each scenario, thanks to Eq. (11), we map the average and the uncertainty of the PM_{2.5} changes due to NH₃ reductions on a regular grid of 0.1° × 0.1° over the studied area. We focus on winter (452 daily predictions for each pixel), which is characterised by high PM_{2.5} concentrations (see Table 2) and the biggest effect of NH₃ (see Table 4).

Considering winter, Figure 6 depicts the average PM_{2.5} reduction for the PRIA scenario, and the associated uncertainty. Analogously, Figure 7 shows the average impact of the Strong scenario. Both scenarios show that in winter, the main reduction effect is obtained in the southeast area of the region where the NH₃ emissions are the highest. In particular, in some areas, the average reduction of PM_{2.5} concentrations is close to 6 μg/m³. Considering the province plain average, Brescia and Cremona, located in the southeast part of the region, show the highest PM_{2.5} reductions of 2-3 μg/m³. On the other hand, highly urbanised lands such as the metropolitan area of Milan, characterised by low levels of NH₃ emissions, do not benefit from the reduction of ammonia emissions. The more marked reduction of NH₃ emissions (Strong scenario) leads to more significant improvements in air quality, achieving local PM_{2.5} reductions average close to 12 μg/m³, reducing the risks associated with the health of the population.



(a)



(b)

Figure 6: PRIA Scenario (-26%). Panel a: average PM_{2.5} reduction in winter, $\bar{\Delta}_p$ (452 daily observations for each pixel). Panel b: uncertainty associated with the average reduction ($\text{std}(\bar{\Delta}_p)$). The pink stars depict the provincial capitals listed in Table 3. The model is only evaluated in non-forested areas below 640 m altitude.

Furthermore, Figure 8 and 9 show the distribution of the winter daily PM_{2.5} reduction aggregated by province and land use for the two scenarios considered. As expected, the largest reductions are obtained in Brescia, Cremona and Mantua provinces, which are characterised by large rural areas and extensive livestock farming. It is also shown that metropolitan and hill areas are not affected by an important reduction.

Table 5 summarises the average of PM_{2.5} reductions aggregated by province in μg/m³. Note that, due to the presence of the Prealps and Alps, the scenario analysis covers a limited surface of the Lecco, Varese, and Como provinces. Finally, Table 6 shows the change aggregated by season. As expected, the largest effect is in winter, when NH₃ plays a limiting role in the formation of PM_{2.5}. We observe that in spring we have no effect as the increase is non-significant being smaller than 0.1% and with a *t*-statistics not larger than 0.125. In winter, when the NH₃ emissions are less abundant, the overall estimated reduction over the plain areas for the PRIA scenario is 1.44 (std = 0.08) while for the Strong scenario is 2.76 (std = 0.16). These

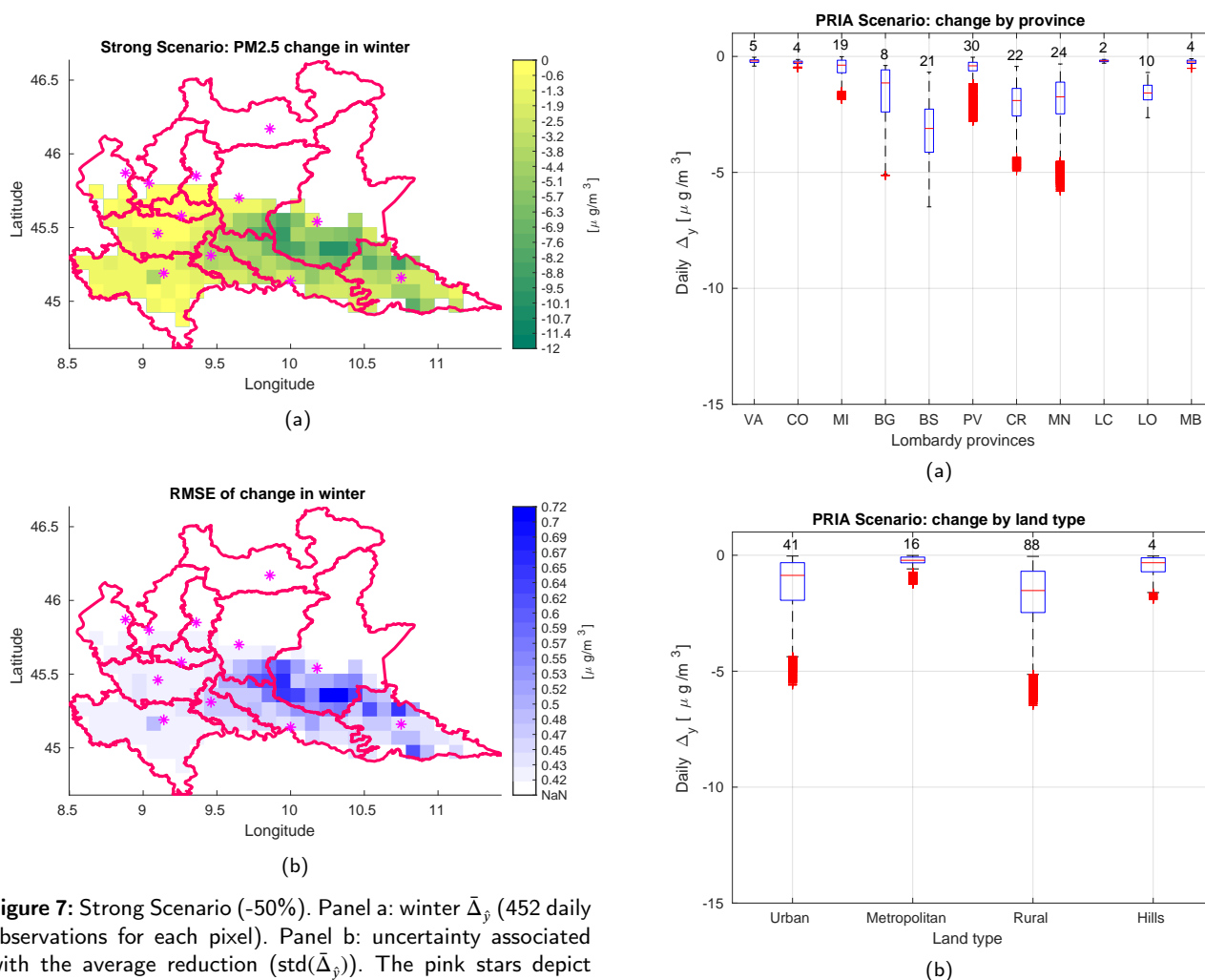


Figure 7: Strong Scenario (-50%). Panel a: winter $\bar{\Delta}_y$ (452 daily observations for each pixel). Panel b: uncertainty associated with the average reduction ($\text{std}(\bar{\Delta}_y)$). The pink stars depict the provincial capitals listed in Table 3. The model is only evaluated in non-forested areas below 640 m altitude.

results can be compared with the PM_{2.5} estimated average 39.49 $\mu\text{g}/\text{m}^3$. So, considering the PRIA scenario, the PM_{2.5} overall reduction is close to 3.5% while considering the Strong scenario, the PM_{2.5} overall reduction is close to 7%.

4. Discussion

This study quantified the reduction in PM_{2.5} concentrations achieved through a reduction in NH₃ emissions for the Lombardy Plain. If we look at the entire area considered and the entire period, against an ammonia emissions reduction of 26% (resulting from the application of the PRIA regional air quality plan), we obtain a significant fine particulate reduction close to 2.4%. A reduction of 50% in ammonia emissions improves the air quality by 4.6%. On the other hand, the absolute reduction in PM_{2.5} depends on the fraction of fine-particulate mass that is directly ammonia-sensitive. In the Lombardy Plain, the composition of PM_{2.5} in winter has a very important secondary component, usually exceeding 50%. As a result, the greatest reductions are obtained in winter (over 3.6% and 7% for the two scenarios, respectively).

Figure 8: Scenario PRIA (-26%). Boxplot of daily Δ_y in winter (452 daily observations for each pixel). Panel a: grouped by province; panel b: grouped by land type. The number of pixels of each category is reported over the corresponding boxplot. The model is evaluated only in the non-forested area under 640 m altitude.

Looking at the spatial distribution of the reductions, it can be seen that the most benefited areas are in the southeastern area of the region, those areas corresponding to the high density of livestock farms and, therefore, ammonia emissions. Consequently, Lombardy has the largest potential of reducing winter averaged PM_{2.5}, considered beneficial to human health, by strongly controlling NH₃ emissions.

5. Conclusions and further developments

The results of this study are generally consistent with those obtained using chemical transport models. Considering the root mean square error, our results are, in some cases, better than [34]. This means that a detailed statistical model fitted to an extensive dataset may catch the main features of a chemical transport model. Since the computational burden is definitely lower, these results hint at the use of statistical emulators for policy impact assessment.

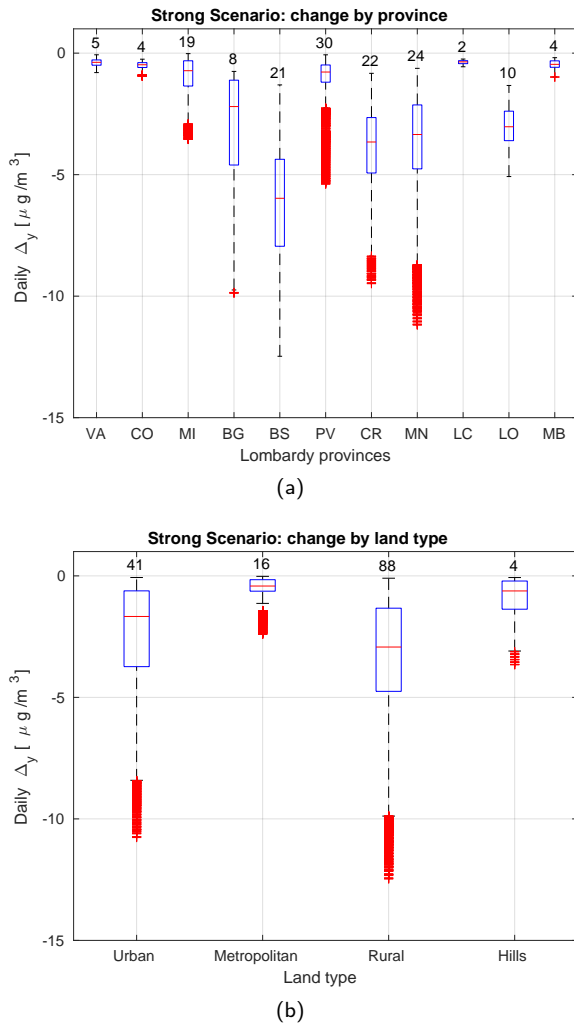


Figure 9: Scenario Strong (-50%). Boxplot of daily $\Delta_{\bar{y}}$ in winter (452 daily observations for each pixel). Panel a: grouped by province; panel b: grouped by land type. The number of pixels of each category is reported over the corresponding boxplot. The model is evaluated only in the non-forested area under 640 m altitude.

Our results are also consistent with those in [9], which are based on observed ammonia concentrations instead of inventory emissions. This means that the emission data are reliable for understanding the impact of livestock on air quality.

From the methodological point of view, our proposal, considering an unstructured skedastic function, may be considered as a first step, opening the development of deterministic and/or stochastic skedastic functions characterised by a smaller number of degrees of freedom. The software for implementing the heteroskedastic HDGM developed in this study represents an updated version of the open-source D-STEM software [35]. It can be accessed on the GitHub repository at <https://github.com/graspa-group/d-stem>.

The monitoring network spatial unbalance mentioned in the introduction and mapped in Figure 2 means that our model has not been trained where NH₃ emissions are very

Table 5

Winter change by province and scenario. D^* is the number of pixels involved in the computation, \bar{y} is the estimated average of the PM_{2.5} concentrations; the columns headed PRIA and Strong show the average reduction and its uncertainty computed using Eq. (13) for both scenarios.

Province	D^*	\bar{y} [$\mu\text{g}/\text{m}^3$]	PRIA [$\mu\text{g}/\text{m}^3$]	Strong [$\mu\text{g}/\text{m}^3$]
VA	5	32.78	-0.19 (0.09)	-0.37 (0.09)
CO	4	36.26	-0.26 (0.11)	-0.50 (0.11)
MI	19	37.56	-0.47 (0.03)	-0.90 (0.06)
BG	8	40.60	-1.62 (0.11)	-3.11 (0.19)
BS	21	47.13	-3.14 (0.18)	-6.04 (0.34)
PV	30	36.10	-0.50 (0.03)	-0.96 (0.06)
CR	22	41.33	-2.04 (0.12)	-3.92 (0.22)
MN	24	39.64	-1.97 (0.11)	-3.80 (0.22)
LC	2	34.50	-0.19 (0.21)	-0.37 (0.21)
LO	10	38.41	-1.57 (0.10)	-3.02 (0.18)
MB	4	37.57	-0.24 (0.11)	-0.46 (0.11)
Overall	149	39.49	-1.44 (0.08)	-2.76 (0.16)

Table 6

PM_{2.5} average change, $\bar{\Delta}_{\bar{y}}(s, t)$, by season and scenario. The number of pixels involved in the computation is $D^* = 149$. \bar{y} is the estimated average of the PM_{2.5} concentrations; the columns headed PRIA and Strong show the average reduction and its uncertainty computed using Eq. (13) and the (%) of reductions for both scenarios.

Season	\bar{y} [$\mu\text{g}/\text{m}^3$]	PRIA		Strong	
		$\mu\text{g}/\text{m}^3$	%	$\mu\text{g}/\text{m}^3$	%
Autumn	24.49	-0.66 (0.07)	-2.68	-1.26 (0.14)	-5.15
Spring	18.57	0.01 (0.08)	0.03	0.01 (0.15)	0.07
Summer	13.92	-0.25 (0.08)	-1.81	-0.49 (0.15)	-3.48
Winter	39.49	-1.44 (0.08)	-3.64	-2.76 (0.16)	-7.00
Overall	24.05	-0.58 (0.04)	-2.42	-1.12 (0.08)	-4.64

high. For this reason, we consider our results cautionary and think that the impact computed may underestimate the true impact. Further research is needed to understand this. Since the Lombardy sampling bias is a consequence of the European Union (EU) rules not requiring NH₃, it is not easy to fill this gap for the EU. One possibility is to validate our approach using Swiss data [14], which has good temporal and spatial coverage.

Credit author statement

Alessandro Fassò: Conceptualisation, Methodology, Supervision. Jacopo Rodeschini: Methodology, Formal analysis, Software, Data curation, Writing original draft. Francesco Finazzi: Methodology, Revision of the article. Alessandro Fusta Moro: Revision of the article.

Acknowledgements

This research was co-funded by Fondazione Cariplo under the grant 2020–4066 “AgrImOnIA: the impact of

agriculture on air quality and the COVID-19 pandemic” from the “Data Science for Science and Society” program and by the European Union - NextGenerationEU, in the framework of the “GRINS - Growing Resilient, INclusive and Sustainable” project (GRINS PE00000018 – CUP F83C22001720001). The views and opinions expressed are solely those of the authors and do not necessarily reflect those of the European Union, nor can the European Union be held responsible for them.

References

- [1] J. S. Benth, F. E. Benth, and P. Jalinskas. A spatial-temporal model for temperature with seasonal variance. *Journal of Applied Statistics*, 34(7):823–841, 2007. doi: 10.1080/02664760701511398. URL <https://doi.org/10.1080/02664760701511398>.
- [2] C. Calulli, A. Fassò, F. Finazzi, A. Pollice, and A. Turnone. Maximum likelihood estimation of the multivariate hidden dynamic geostatistical model with application to air quality in Apulia, Italy. *Environmetrics*, 26(6):406–417, 2015.
- [3] A. Clappier, P. Thunis, M. Beekmann, J. Putaud, and A. de Meij. Impact of SO_x, NO_x and NH₃ emission reductions on PM_{2.5} concentrations across Europe: Hints for future measure development. *Environment International*, 156:106699, 2021.
- [4] N. Cressie and C. K. Wikle. *Statistics for spatio-temporal data*. John Wiley & Sons, 2015.
- [5] N. Cressie, T. Shi, and E. L. Kang. Fixed rank filtering for spatio-temporal data. *Journal of Computational and Graphical Statistics*, 19(3):724–745, 2010.
- [6] A. De Meij, P. Thunis, B. Bessagnet, and C. Cuvelier. The sensitivity of the chimere model to emissions reduction scenarios on air quality in Northern Italy. *Atmospheric environment*, 43(11):1897–1907, 2009.
- [7] R. F. Engle. Autoregressive conditional heteroscedasticity with estimates of the variance of United Kingdom inflation. *Econometrica*, 50(4):987–1007, 1982. ISSN 00129682, 14680262. URL <http://www.jstor.org/stable/1912773>.
- [8] European Environment Agency (EEA). Premature deaths due to exposure to fine particulate matter in Europe (8th EAP), 2022. URL <https://www.eea.europa.eu/ims/health-impacts-of-exposure-to>.
- [9] A. Fassò. To what extent airborne particulate matters are influenced by ammonia and nitrogen oxides? *arXiv preprint arXiv:2310.09302*, 2023.
- [10] A. Fassò and M. Cameletti. A unified statistical approach for simulation, modeling, analysis and mapping of environmental data. *Simulation*, 86(3):139–153, 2010.
- [11] A. Fassò, J. Rodeschini, A. Fusta Moro, Q. Shaboviq, P. Maranzano, M. Cameletti, F. Finazzi, N. Golini, R. Ignaccolo, and P. Otto. AgrImOnIA: Open Access dataset correlating livestock and air quality in the Lombardy region, Italy, May 2023. URL <https://doi.org/10.5281/zenodo.7956006>.
- [12] A. Fassò, J. Rodeschini, A. F. Moro, Q. Shaboviq, P. Maranzano, M. Cameletti, F. Finazzi, N. Golini, R. Ignaccolo, and P. Otto. Agrimonia: a dataset on livestock, meteorology and air quality in the Lombardy region, Italy. *Scientific Data*, 2023. doi: 10.1038/s41597-023-02034-0.
- [13] C. Francq and J.-M. Zakoian. *GARCH models: structure, statistical inference and financial applications*. John Wiley & Sons, 2019.
- [14] S. K. Grange, J. Sintermann, and C. Hueglin. Meteorologically normalised long-term trends of atmospheric ammonia (NH₃) in Switzerland/Liechtenstein and the explanatory role of gas-aerosol partitioning. *Science of The Total Environment*, 900:165844, 2023. ISSN 0048-9697. doi: <https://doi.org/10.1016/j.scitotenv.2023.165844>. URL <https://www.sciencedirect.com/science/article/pii/S0048969723044698>.
- [15] M. J. Heaton, A. Datta, A. O. Finley, R. Furrer, J. Guinness, R. Guhaniyogi, F. Gerber, R. B. Gramacy, D. Hammerling, M. Katzfuss, F. Lindgren, D. Nychka, F. Sun, and A. Zammit-Mangion. A case study competition among methods for analyzing large spatial data. *Journal of Agricultural, Biological and Environmental Statistics*, 24(3):398–425, 2019. doi: 10.1007/s13253-018-00348-w.
- [16] H.-C. Huang and N. Cressie. Spatio-temporal prediction of snow water equivalent using the Kalman filter. *Computational Statistics & Data Analysis*, 22(2):159–175, 1996.
- [17] C. M. Hulshof and M. N. Umana. Power laws and plant trait variation in spatio-temporally heterogeneous environments. *Global Ecology and Biogeography*, 32(2):310–323, 2023. doi: <https://doi.org/10.1111/geb.13620>. URL <https://onlinelibrary.wiley.com/doi/abs/10.1111/geb.13620>.
- [18] A. Inness, M. Ades, A. Agustí-Panareda, J. Barré, A. Benedictow, A.-M. Blechschmidt, J. J. Dominguez, R. Engelen, H. Eskes, J. Flemming, V. Huijnen, L. Jones, Z. Kipling, S. Massart, M. Parrington, V.-H. Peuch, M. Razinger, S. Remy, M. Schulz, and M. Suttie. The CAMS reanalysis of atmospheric composition. *Atmos. Chem. Phys.*, 19(6):3515–3556, 2019. doi: <https://doi.org/10.5194/acp-19-3515-2019>. URL <https://acp.copernicus.org/articles/19/3515/2019/>.
- [19] M. Jurek and M. Katzfuss. Scalable spatio-temporal smoothing via hierarchical sparse Cholesky decomposition. *Environmetrics*, 34(1):e2757, 2023. doi: <https://doi.org/10.1002/env.2757>. URL <https://onlinelibrary.wiley.com/doi/abs/10.1002/env.2757>.
- [20] G. Lonati and S. Cernuschi. Temporal and spatial variability of atmospheric ammonia in the Lombardy region (Northern Italy). *Atmospheric Pollution Research*, 11(12):2154–2163, 2020.
- [21] D. Lovarelli, D. Fugazza, M. Costantini, C. Conti, G. Diolaiuti, and M. Guarino. Comparison of ammonia air concentration before and during the spread of COVID-19 in Lombardy (Italy) using ground-based and satellite data. *Atmospheric Environment*, 259:118534, 2021.
- [22] A. Megaritis, C. Fountoukis, P. Charalampidis, C. Pilinis, and S. N. Pandis. Response of fine particulate matter concentrations to changes of emissions and temperature in Europe. *Atmospheric Chemistry and Physics*, 13(6):3423–3443, 2013.
- [23] J. Mur and A. Angulo. Model selection strategies in a spatial setting: Some additional results. *Regional Science and Urban Economics*, 39(2):200–213, 2009. ISSN 0166-0462. doi: <https://doi.org/10.1016/j.regsciurbeco.2008.05.018>. URL <https://www.sciencedirect.com/science/article/pii/S0166046208001051>.
- [24] G. Nowak and A. Welsh. Improved prediction for a spatio-temporal model. *Environmental and Ecological Statistics*, 27:631–648, 2020.
- [25] P. Otto and W. Schmid. A general framework for spatial GARCH models. *Statistical Papers*, 64(5):1721–1747, 2023. ISSN 1613-9798. doi: 10.1007/s00362-022-01357-1. URL <https://doi.org/10.1007/s00362-022-01357-1>.
- [26] P. Otto, W. Schmid, and R. Garthoff. Generalised spatial and spatiotemporal autoregressive conditional heteroscedasticity. *Spatial Statistics*, 26:125–145, 2018. ISSN 2211-6753. doi: <https://doi.org/10.1016/j.spasta.2018.07.005>. URL <https://www.sciencedirect.com/science/article/pii/S2211675318300794>.
- [27] P. Otto, A. F. Moro, J. Rodeschini, Q. Shaboviq, R. Ignaccolo, N. Golini, M. Cameletti, P. Maranzano, F. Finazzi, and A. Fassò. Spatiotemporal modelling of PM_{2.5} concentrations in Lombardy (Italy) – a comparative study, 2023.
- [28] L. Padilla, B. Lagos-Álvarez, J. Mateu, and E. Porcu. Space-time autoregressive estimation and prediction with missing data based on Kalman filtering. *Environmetrics*, 31(7):e2627, 2020. doi: <https://doi.org/10.1002/env.2627>. URL <https://onlinelibrary.wiley.com/doi/abs/10.1002/env.2627>.
- [29] A. Pozzer, A. P. Tsimpidi, V. A. Karydis, A. De Meij, and J. Lelieveld. Impact of agricultural emission reductions on fine-particulate matter and public health. *Atmospheric Chemistry and Physics*, 17(20):12813–12826, 2017.
- [30] J. Rougier, A. Brady, J. Bamber, S. Chuter, S. Royston, B. D. Vishwakarma, R. Westaway, and Y. Ziegler. The scope of the Kalman filter for spatio-temporal applications in environmental science. *Environmetrics*, 34(1):e2773, 2023. doi: <https://doi.org/10.1002/env.2773>.

- URL <https://onlinelibrary.wiley.com/doi/abs/10.1002/env.2773>.
- [31] H. Rue, S. Martino, and N. Chopin. Approximate Bayesian inference for latent Gaussian models by using integrated nested Laplace approximations. *Journal of the Royal Statistical Society Series B: Statistical Methodology*, 71(2):319–392, 2009.
- [32] R. H. Shumway, D. S. Stoffer, and D. S. Stoffer. *Time series analysis and its applications*, volume 3. Springer, 2000.
- [33] B. J. Smith, J. Yan, and M. K. Cowles. Unified geostatistical modeling for data fusion and spatial heteroskedasticity with R package ramps. *Journal of Statistical Software*, 25(10), 2008. doi: 10.18637/jss.v025.i10. URL <https://www.jstatsoft.org/index.php/jss/article/view/v025i10>.
- [34] G. Veratti, M. Stortini, R. Amorati, L. Bressan, G. Giovannini, S. Bande, F. Bissardella, S. Ghigo, E. Angelino, L. Colombo, et al. Impact of NO_x and NH₃ emission reduction on particulate matter across Po Valley: A LIFE-IP-PREPAIR study. *Atmosphere*, 14(5): 762, 2023.
- [35] Y. Wang, F. Finazzi, and A. Fassò. D-STEM v2: A software for modeling functional spatio-temporal data. *Journal of Statistical Software*, 99(10):1–29, 2021. doi: 10.18637/jss.v099.i10. URL <https://www.jstatsoft.org/index.php/jss/article/view/v099i10>.
- [36] Y. Zhang, S. X. Chen, and L. Bao. Air pollution estimation under air stagnation—a case study of Beijing. *Environmetrics*, 34(6): e2819, 2023. doi: <https://doi.org/10.1002/env.2819>. URL <https://onlinelibrary.wiley.com/doi/abs/10.1002/env.2819>.
- [37] X. Zheng, B. Guo, J. He, and S. X. Chen. Effects of corona virus disease-19 control measures on air quality in North China. *Environmetrics*, 32(2):e2673, 2021. doi: <https://doi.org/10.1002/env.2673>. URL <https://onlinelibrary.wiley.com/doi/abs/10.1002/env.2673>.